Research Article Vol. 32, No. 3 / 29 Jan 2024 / Optics Express 3221
Optics EXPRESS

Growth, spectroscopy and SESAM mode-locking of a "mixed" Yb:Ca(Gd,Y)AlO_4 disordered crystal

Peixiong Zhang,[1] Wenjie Wu,[1] Zhang-Lang Lin,[2] Zhi-Qiang Li,[2] Pavel Loiko,[3] Simone Normani,[3] Zhenqiang Chen,[1] Zhen Li,[1] Ghassen Zin Elabedine,[4] Xavier Mateos,[4] Huang-Jun Zeng,[2] Ge Zhang,[2] Hai-Yu Nie,[2] Alain Braud,[4] Patrice Camy,[4] Valentin Petrov,[5] and Weidong Chen[2,5,*]

[1]*Department of Optoelectronic Engineering, Jinan University, 510632 Guangzhou, China*
[2]*Fujian Institute of Research on the Structure of Matter, Chinese Academy of Sciences, 350002 Fuzhou, China*
[3]*Centre de Recherche sur les Ions, les Matériaux et la Photonique (CIMAP), UMR 6252 CEA-CNRS-ENSICAEN, Université de Caen, 6 Boulevard Maréchal Juin, 14050 Caen Cedex 4, France*
[4]*Universitat Rovira i Virgili, URV, Física i Cristal·lografia de Materials (FiCMA)- Marcel·lí Domingo 1, 43007 Tarragona, Spain*
[5]*Max Born Institute for Nonlinear Optics and Short Pulse Spectroscopy, Max-Born-Str. 2a, 12489 Berlin, Germany*
[*]*chenweidong@fjirsm.ac.cn*

Abstract: We present the growth, spectroscopy, continuous-wave (CW) and passively mode-locked (ML) operation of a novel "mixed" tetragonal calcium rare-earth aluminate crystal, Yb^{3+}:Ca(Gd,Y)AlO_4. The absorption, stimulated-emission, and gain cross-sections are derived for π and σ polarizations. The laser performance of a ***c***-cut Yb:Ca(Gd,Y)AlO_4 crystal is studied using a spatially single-mode, 976-nm fiber-coupled laser diode as a pump source. A maximum output power of 347 mW is obtained in the CW regime with a slope efficiency of 48.9%. The emission wavelength is continuously tunable across 90 nm (1010 – 1100 nm) using a quartz-based Lyot filter. With a commercial SEmiconductor Saturable Absorber Mirror to initiate and maintain ML operation, soliton pulses as short as 35 fs are generated at 1059.8 nm with an average output power of 51 mW at ~65.95 MHz. The average output power can be scaled to 105 mW for slightly longer pulses of 42 fs at 1063.5 nm.

1. Introduction

Ytterbium (Yb^{3+}) doped tetragonal rare-earth calcium aluminates, denoted as Yb:Ca*RE*AlO_4, where *RE* represents either Gd or Y, have gained prominence as exceptional laser materials. These crystals exhibit remarkable capabilities for power-scalable, broadly tunable and ultrafast lasers operating at ~1 μm [1–3]. In the literature, the Gd and Y compounds are frequently abbreviated as Yb:CALGO and Yb:CALYO, respectively. The Ca*RE*AlO_4 crystals are optically uniaxial and belong to the family of compounds with a general chemical formula of $ABCO_4$, where A = Ca or Sr, B = Y or lanthanide (*Ln*) ion, and C = Al or Ga. When Yb^{3+} replaces for the RE^{3+} host-forming cations in a crystallographic site exhibiting point symmetry C_{4v} and IX-fold oxygen coordination, this site is statistically occupied by both Ca^{2+} and Yb^{3+}|RE^{3+} ions [4]. The ease of Yb^{3+} doping in Ca*RE*AlO_4 crystals is attributed to the availability of passive *RE* sites. The inhomogeneous spectral broadening in these crystals stems from the second coordination sphere of the dopant Yb^{3+} ions, influenced by the random distribution of Ca^{2+} and RE^{3+} ions.

#514436 https://doi.org/10.1364/OE.514436
Journal © 2024 Received 11 Dec 2023; revised 28 Dec 2023; accepted 29 Dec 2023; published 16 Jan 2024

Optics EXPRESS

It is due to the charge disparity between these ions and varying cation-cation distances within this coordination sphere. Consequently, the Yb^{3+} ions in Yb:Ca*RE*AlO_4 display a "glassy"-like spectroscopic behavior, characterized by rather broad absorption and emission bands [4]. The broad, smooth and flat gain profiles of the Yb:Ca*RE*AlO_4 crystals are particularly advantageous for widely tunable laser operation and achieving sub-50 fs pulse generation through passive mode-locking [5–14]. In combination with the Kerr-lens mode-locking technique, even sub-20 fs pulses can be generated using such crystals [15,16]. In contrast to the widely recognized disordered cubic garnets, another material family attractive for femtosecond mode-locked (ML) laser at ~1 μm, whose thermal conductivity is comparable to that of glasses, the disordered Ca*RE*AlO_4 crystals exhibit relatively high thermal conductivity, particularly noteworthy in the case of $CaGdAlO_4$ with an average value of ~6.7 $Wm^{-1}K^{-1}$ for 2 at.% Yb [17]. Significantly, this thermal conductivity exhibits a moderate dependence on the Yb^{3+} doping level [17]. The Yb:Ca*RE*AlO_4 crystals also feature attractive thermo-optical properties, namely, positive thermal lensing with a weak refractive power and astigmatism (a nearly athermal behavior) owing to negative dn/dT coefficients [17,18]. It is worth noting that the emission of Yb:Ca*RE*AlO_4 lasers is linearly polarized due to their strong intrinsic birefringence [19] and the noticeable anisotropy of the gain cross sections.

Furthermore, the structural disorder present in the Ca*RE*AlO_4 compounds can be augmented by compositional disorder, resulting in additional inhomogeneous spectral broadening. This contributes to smoothing and flattening of the gain profiles of the Yb^{3+} dopant. The engineering of compositional disorder in the passive host can be accomplished by mixing Gd^{3+} and Y^{3+} in the growth melt [20] (as there exists an isostructural series of solid-solution compositions $CaGd_{1-x}Y_xAlO_4$ for the entire range of $0 < x < 1$) or by introducing Lu^{3+} to either of these compounds [21–23] (there exists a limit for Lu^{3+} solubility, as the tetragonal compound $CaLuAlO_4$ is not stable [22,24]). ML Yb-laser operation based on such a calcium aluminate crystal with additional compositional disorder was reported for the first time in [21]. However, Lu-doping of CALGO as low as 2.6 at.% [21] is comparable with the active ion (Yb) concentration and is not expected to contribute significantly to the compositional disorder. It is similar to the effect of the active ion doping in any laser crystal where the term disorder is not used because of the smallness of the effect.

The Ca*RE*AlO_4 crystals feature congruent melting, simplifying the process of large crystal growth by the conventional Czochralski (Cz) method [25,26]. In the present work, our objective was to explore the polarized spectroscopic properties, and continuous-wave (CW) and ML laser operation of a newly developed Yb^{3+}-doped "mixed" tetragonal rare-earth calcium aluminate, Ca(Gd,Y)AlO_4, representing a solid-solution between CALGO and CALYO. Mixing host crystals containing the optically passive Gd^{3+} and Y^{3+} ions provide more flexibility for engineering the compositional disorder and the resulting spectral gain profiles compared to doping with Lu^{3+} which is limited to relatively low levels [21].

2. Crystal growth

The Yb:Ca(Gd,Y)AlO_4 crystal was grown using the conventional Cz method with 5 at.% Yb^{3+} content in the melt. Yb^{3+}-doped Ca(Gd,Y)AlO_4 polycrystalline tablets were first synthesized through the solid-state reaction method. The raw materials used were $CaCO_3$, Gd_2O_3, Yb_2O_3, Y_2O_3 and Al_2O_3, each possessing a purity level of 99.999%. The corresponding equation for the solid-state reaction is as follows:

$$CaCO_3+0.025Yb_2O_3+0.165Gd_2O_3+0.31Y_2O_3+0.5Al_2O_3 \rightarrow CaGd_{0.33}Yb_{0.05}Y_{0.62}AlO_4+CO_2\uparrow$$

The powders were weighed and stirred for 48 h to ensure their uniform mixing, then pressed into tablets with a diameter of 60 mm. A muffle furnace was used for sintering at 1350°C for 36 h in air. After that, the synthesized polycrystalline charge was transferred into an Ir crucible with a

Optics EXPRESS

diameter of 70 mm. The single crystal was grown using an [001] oriented seed from an undoped CALYO crystal under nitrogen atmosphere. The pulling rate and the rotation speed of the seed were set to 0.6 - 1.0 mm/h and 12 - 18 rpm, respectively. The grown crystal was slowly cooled down to room temperature (RT) at a rate of 30 ~ 50°C/h. Figure 1 shows a photograph of the as-grown Yb:Ca(Gd,Y)AlO_4 crystal with dimensions of $\Phi 40 \times 60$ mm^3. No cracks, inclusions, or bubbles are seen.

Fig. 1. A photograph of the as-grown Yb:Ca(Gd,Y)AlO_4 crystal boule, the growth direction is along the [001] axis.

The actual composition was determined by Inductively Coupled Plasma Mass Spectrometry (ICP-MS) to be $CaGd_{0.448}Yb_{0.032}Y_{0.520}AlO_4$, where the Yb^{3+} doping concentration is 3.2 at.% (Yb^{3+} ion density: $N_{Yb} = 3.6 \times 10^{-20}$ cm^{-3}), corresponding to a segregation coefficient of 0.64. According to an X-ray powder diffraction study, the grown crystal is of single-phase nature. Yb:Ca(Gd,Y)AlO_4 belongs to the tetragonal class (sp. gr. $D^{17}_{4\,h}$ - *I*4/*mmm*, No. 139) exhibiting a K_2NiF_4 type structure and it is isostructural to the parent compound, Yb:$CaYAlO_4$. Yb:Ca(Gd,Y)AlO_4 is optically uniaxial (the optical axis is parallel to the ***c***-axis) and the two principal light polarizations are $\boldsymbol{E} \parallel \boldsymbol{c}$ (π) and $\boldsymbol{E} \perp \boldsymbol{c}$ (σ).

3. Optical spectroscopy

The factor group analysis for the primitive cell of the $D^{17}_{4\,h}$ symmetry predicts the following set of irreducible representations at the center of the Brillouin zone ($\boldsymbol{k} = 0$): $\Gamma = 2A_1\,g + 2E_g + 4A_{2u} + 5E_u + B_{2u}$ [27,28]. Out of them, four modes are Raman active ($2A_1\,g + 2E_g$), seven modes are IR active ($3A_{2u} + 4E_u$), two modes ($A_{2u} + E_u$) are acoustic and one (B_{2u}) is silent [28]. The polarized Raman spectra of an ***a***-cut Yb:Ca(Gd,Y)AlO_4 crystal measured in the $\boldsymbol{a}(ij)\bar{\boldsymbol{a}}$, i and $j = \pi$ and σ, geometries are shown in Fig. 2(a) (here, we use Porto's notations [29]).

The Raman spectra are strongly polarized. For the studied geometries, all the Raman-active modes appear: the $\boldsymbol{a}(\pi\pi)\bar{\boldsymbol{a}}$ geometry selects the $A_1\,g$ phonons at 321 and 525/556 cm^{-1}, and in the $\boldsymbol{a}(\pi\sigma)\bar{\boldsymbol{a}}$ one, the E_g modes appear at ~160 and 317 cm^{-1}. The dominant band at 321 cm^{-1} is thus assigned to Ca|RE vibrations along the [001] axis and the high-frequency band at 525/556 cm^{-1}with a complex structure – to O vibrations. The bands at ~618 and 651 cm^{-1} are probably due to defect-induced modes.

The Raman spectra of the "mixed" Yb:Ca(Gd,Y)AlO_4 and parent Yb:$CaYAlO_4$ crystals measured in the $\boldsymbol{a}(\pi\pi)\bar{\boldsymbol{a}}$ geometry are very close, Fig. 2(b), indicating a small red-shift in the peak position for the solid-solution crystal composition.

The RT absorption and emission properties of the Yb:Ca(Gd,Y)AlO_4 crystal were studied for the two principal light polarizations, π and σ and compared with those for the parent compound, Yb:$CaYAlO_4$. Figure 3(a) shows the absorption cross-section (σ_{abs}) spectra for the $^2F_{7/2} \rightarrow {}^2F_{5/2}$ transition of Yb^{3+} ions. For the "mixed" crystal, the maximum value of σ_{abs} reaches 4.46×10^{-20} cm^2 at 979.7 nm (zero-phonon line, ZPL) with a bandwidth (full width at half maximum, FWHM) of the absorption peak of 9.4 nm for π-polarized light. In the case of σ-polarization, the peak σ_{abs} value is lower, 1.85×10^{-20} cm^2 at 979.8 nm, while the absorption bandwidth is similar, 9.1 nm. The broad ZPL absorption bandwidth for both light polarizations mitigates the restrictions on the use of commercially available high-power InGaAs laser diodes emitting at ~980 nm. This

Optics EXPRESS

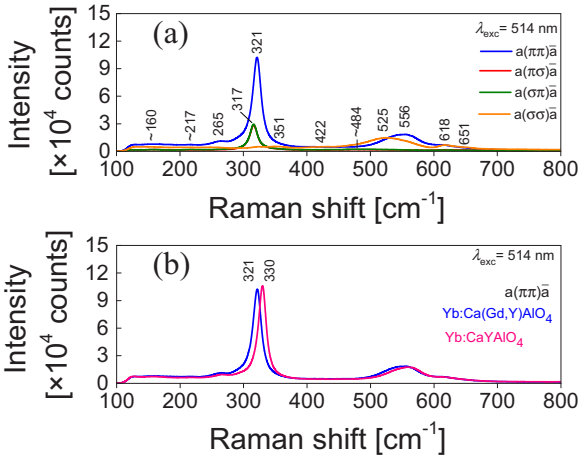

Fig. 2. RT polarized Raman spectra of Yb:Ca(Gd,Y)AlO_4: (a) $\boldsymbol{a}(ij)\bar{\boldsymbol{a}}$, where $i, j = \pi$ and σ geometries (Porto's notations); (b) a comparison of Raman spectra of Yb:Ca(Gd,Y)AlO_4 and Yb:$CaYAlO_4$ [$\boldsymbol{a}(\pi\pi)\bar{\boldsymbol{a}}$ geometry]. $\lambda_{exc} = 514$ nm.

is particularly relevant in addressing potential temperature-induced drift in the diode emission wavelength.

The luminescence spectra of both the "mixed" Yb:Ca(Gd,Y)AlO_4 and parent Yb:$CaYAlO_4$ crystals are presented in Fig. 3(b). The spectra are strongly polarized. The effect of Gd^{3+} addition

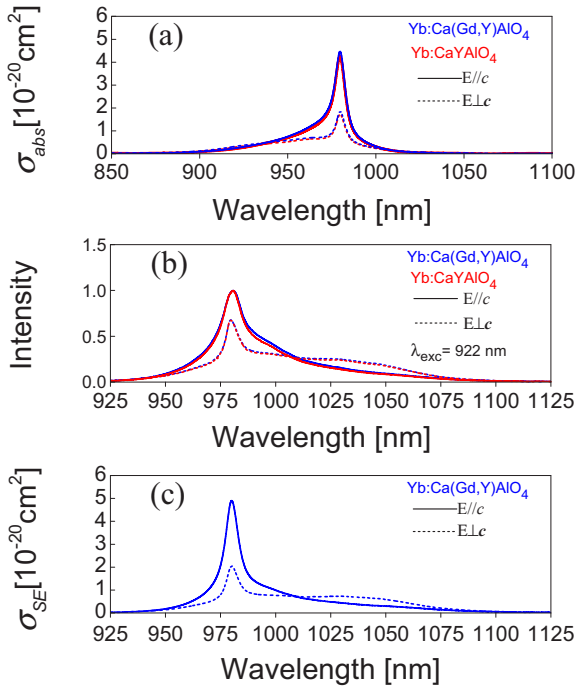

Fig. 3. RT polarized absorption and emission properties of Yb^{3+} ions in the Ca(Gd,Y)AlO_4 and $CaYAlO_4$ crystals: (a) absorption cross-section (σ_{abs}) spectra; (b) luminescence spectra, $\lambda_{exc} = 922$ nm; (c) stimulated-emission (σ_{SE}) cross-sections, Yb:Ca(Gd,Y)AlO_4. Light polarizations: $\boldsymbol{E} \parallel \boldsymbol{c}$ (π) and $\boldsymbol{E} \perp \boldsymbol{c}$ (σ).

Optics EXPRESS

to the crystal composition is revealed by an additional spectral broadening and a red shift of the Yb^{3+} emission band. The stimulated-emission (SE, σ_{SE}) cross-sections were calculated using a combination of the Füchtbauer–Ladenburg (F-L) formula and the reciprocity method (RM). A satisfactory agreement between the two methods was achieved for a radiative lifetime of the $^2F_{5/2}$ Yb^{3+} excited manifold of 0.41 ± 0.03 ms. The refractive indices of the "mixed" crystal were calculated based on the Sellmeier equations [30] assuming a linear variation of the refractive index in the $CaY_{1-x}Gd_xAlO_4$ substitutional solid-solution yielding $n_o = 1.902$ and $n_e = 1.925$ at ~1 μm for the ordinary and extraordinary rays, respectively.

The resulting σ_{SE} spectra are depicted in Fig. 3(c). In the spectral range where positive gain and lasing are expected (i.e., at wavelengths significantly above the ZPL), the SE cross-section is 0.25×10^{-20} cm^2 at ~1057 nm for π-polarization. Conversely, for σ-polarization, the peak σ_{SE} is 0.61×10^{-20} cm^2 at ~1049 nm. The inherent anisotropy observed in the SE cross-sections suggests that Yb:Ca(Gd,Y)AlO_4 lasers based on ***a***-cut crystals are likely to emit linearly polarized light without the need for additional polarization-selective elements.

The RT luminescence lifetime of the upper laser level ($^2F_{5/2}$) of Yb^{3+} ions in Ca(Gd,Y)AlO_4 was determined by studying a finely powdered crystalline sample to reduce the impact of radiation trapping (reabsorption) on the measured kinetics, Fig. 4. The Yb^{3+} ion luminescence shows a single-exponential decay with a characteristic lifetime $\tau_{lum.}$ of 705 μs. For Yb^{3+} ions in the parent crystal $CaYAlO_4$, $\tau_{lum.} = 675$ μs. These values exceed the estimate of the radiative lifetime most probably due to the residual effect of reabsorption.

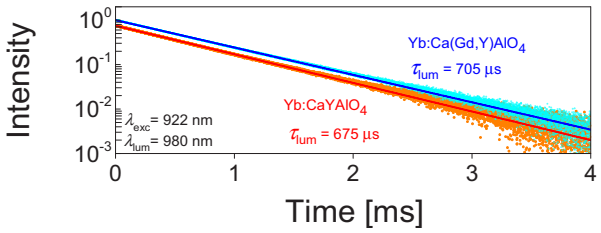

Fig. 4. RT luminescence decay curves of the 3.2 at.% Yb:Ca(Gd,Y)AlO_4 and 3.7 at.% Yb:$CaYAlO_4$ crystals, $\lambda_{exc} = 922$ nm, $\lambda_{lum} = 980$ nm, *circles* – experimental data, *lines* – single-exponential fits.

Adhering to the quasi-three-level nature of the Yb laser scheme with reabsorption, the polarized gain cross-sections, $\sigma_{gain} = \beta\sigma_{SE} - (1 - \beta)\sigma_{abs}$, of Yb^{3+}:Ca(Gd,Y)AlO_4 were determined for the two principal polarizations, π and σ, as illustrated in Fig. 5. Here, $\beta = N_2/N_{Yb}$ represents the inversion ratio, where N_2 corresponds to the population of the upper laser level ($^2F_{5/2}$). The "glassy-like" gain profiles stem from pronounced inhomogeneous spectral line broadening induced by both the structural and compositional disorder, as well as homogeneous temperature broadening. The gain spectra extend well beyond the range of electronic transitions, which is attributed to a significant phonon sideband related to a strong lattice-orbit interaction in Ca*RE*AlO_4 crystals. As the inversion ratio increases, the spectral maximum undergoes a blue shift, from ~1055 nm at low ($\beta = 0.07$) to 1017 nm at a higher ($\beta = 0.3$) inversion ratio for π-polarization, and from ~1053 nm to 1034 nm for σ-polarization. For $\beta = 0.3$, the gain bandwidth (FWHM) is about 67 nm for π-polarization, and ~62 nm for σ-polarization. This broadband gain behavior underscores the high potential of Yb:Ca(Gd,Y)AlO_4 for wide wavelength tuning and the generation of sub-50 fs pulses via passive mode-locking.

The low-temperature (LT, 12 K) absorption and emission spectra of Yb^{3+} ions in the "mixed" Yb:Ca(Gd,Y)AlO_4 and parent Yb:$CaYAlO_4$ crystals were measured with polarized light to determine the crystal-field splitting, see Fig. 6(a) and (b). In Yb:Ca(Gd,Y)AlO_4, the host-forming Ca^{2+} and $Gd^{3+}|Y^{3+}$ cations are statistically distributed over the same lattice sites (Wyckoff: 4*e*)

Optics EXPRESS

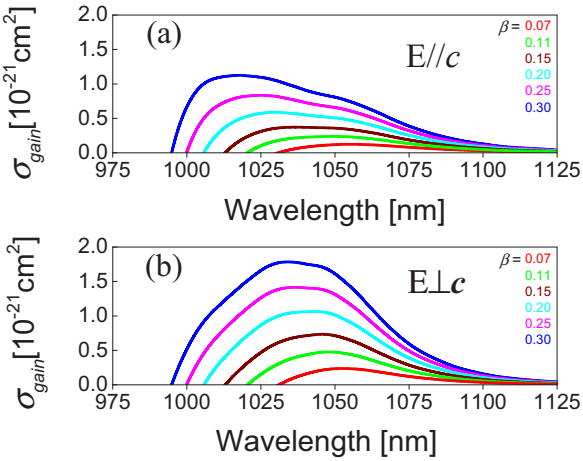

Fig. 5. RT polarized gain cross-section (σ_{gain}) spectra of Yb:Ca(Gd,Y)AlO_4, $\sigma_{gain} = \beta\sigma_{SE} - (1-\beta)\sigma_{abs}$, $\beta = N_2(^2F_{5/2})/N_{Yb}$ – population inversion ratio. The light polarization is (a) $\boldsymbol{E} \parallel \boldsymbol{c}$ (π) and (b) $\boldsymbol{E} \perp \boldsymbol{c}$ (σ).

of the C_{4v} symmetry and they are IX-fold oxygen coordinated. The $^2F_{7/2}$ and $^2F_{5/2}$ manifolds of Yb^{3+} ions will be split by the crystal-field into 4 and 3 Stark components, respectively, which are numbered in the present work as 0 – 3 ($^2F_{7/2}$) and 0' – 2' ($^2F_{5/2}$). The LT spectra of Yb^{3+} ions reveal a strong inhomogeneous spectral line broadening arising from the varying composition of the second coordination sphere around the active ions composed of both Ca^{2+} and $Gd^{3+}|Y^{3+}$ cations [23].

For the Ca(Gd,Y)AlO_4 crystal, the Yb^{3+} zero-phonon line (the 0 ↔ 0' transition) has an energy E_{ZPL} of 10190 cm^{-1} and the total splitting of the ground-state, $\Delta E(^2F_{7/2})$, is 631 cm^{-1}. The experimental crystal-field splitting of Yb^{3+} ions in this crystal is shown on the inset of Fig. 6(b).

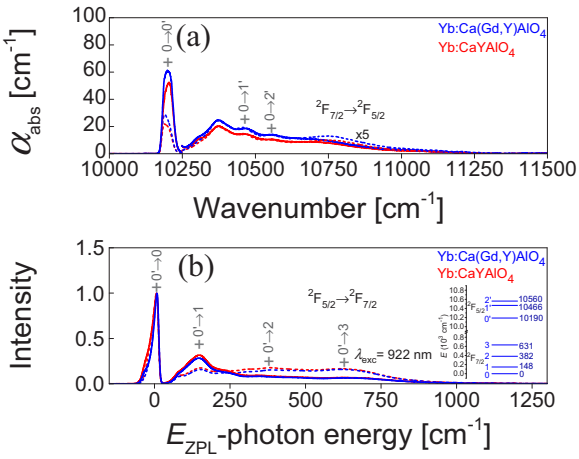

Fig. 6. Low-temperature (12 K) polarized (a) absorption and (b) luminescence spectra of Yb^{3+} ions in the Yb:Ca(Gd,Y)AlO_4 and Yb:$CaYAlO_4$ crystals. Light polarizations: π and σ. "+" mark the electronic transitions. *Inset* in (b) – experimental crystal-field splitting for Yb^{3+} ions in the "mixed" crystal. ×5 means that the luminescence spectra in the range of 10250 - 15000 cm^{-1} are multiplied by a factor of 5.

Optics EXPRESS

Here, for the assignment of electronic transitions, we followed the theoretical crystal-field calculation by Hutchinson *et al.* [31]. The partition functions for the lower (l) and upper (u) Yb^{3+} manifolds are $Z_l = 1.680$ and $Z_u = 1.419$ and their ratio Z_l/Z_u is 1.184 (at RT). The effect of Gd^{3+} addition to the crystal composition is relatively weak but is clearly observed in the additional broadening of electronic transitions and a slight shift of the ZPL peak position.

4. Laser set-up

The schematic of the Yb:Ca(Gd,Y)AlO_4 laser is depicted in Fig. 7. An 3-mm thick uncoated laser sample with 3.2 at.% Yb^{3+} dopant was cut from the as-grown bulk to facilitate light propagation along the crystallographic ***c***-axis (***c***-cut). It had an aperture of 4×4 mm^2, and was polished both sides to laser-grade quality with good parallelism and left uncoated. The sample was mounted in a copper holder without active cooling and positioned at Brewster's angle between two concave folding mirrors, M_1 and M_2 (radius of curvature, RoC = -100 mm), in an astigmatically compensated X-folded linear cavity. The pump source was a fiber-coupled InGaAs laser diode, providing a maximum incident power of 1.33 W at 976 nm (unpolarized radiation). Its emission wavelength was stabilized by a fiber Bragg grating (FBG), resulting in an emission linewidth (FWHM) of ~0.2 nm. The measured pump beam quality factor (M^2) at the maximum output power was ~1.02. Collimation and focusing into the laser crystal through the pump mirror (M_1) were realized using an aspherical lens L_1 ($f = 26$ mm) and a spherical lens L_2 ($f = 75$ mm). This resulted in a beam waist (radius) of 14.3 µm × 32.3 µm in the sagittal and tangential planes, respectively.

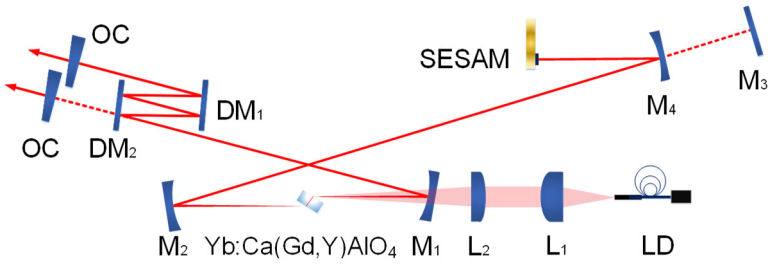

Fig. 7. Schematic of the diode-pumped Yb:Ca(Gd,Y)AlO_4 laser. LD: fiber-coupled laser diode; L_1: aspherical lens; L_2: spherical lens; M_1, M_2 and M_4: curved mirrors (RoC = -100 mm); M_3: flat rear mirror for CW laser operation; DM_1 and DM_2: flat dispersive mirrors; OC: output coupler; SESAM: SEmiconductor Saturable Absorber Mirror.

The CW laser performance was assessed in a four-mirror cavity configuration without incorporating the SEmiconductor Saturable Absorber Mirror (SESAM) and the dispersive mirrors (DMs). One arm of the cavity was terminated by a flat rear mirror, M_3, while the other arm ended with a plane-wedged output coupler (OC) with a transmission at the laser wavelength (T_{OC}) ranging from 0.4% to 7.5%. Using the ABCD matrix method, the radius of the fundamental laser cavity mode within the Yb:Ca(Gd,Y)AlO_4 crystal was estimated to be 21 µm × 38 µm in the sagittal and tangential planes, respectively. The single-pass pump absorption, measured under lasing conditions, exhibited a marginal reduction from 69.6% to 65% with increasing T_{OC} due to the decreasing recycling effect.

A curved mirror M_4 (RoC = -100 mm) replaced the flat rear mirror M_3 so as to create a secondary beam waist on the saturable absorber (SA) with a beam radius of ~81 µm for efficient bleaching. A commercial SESAM (BATOP, GmbH) was implemented as SA to initiate and stabilize ML operation. Its parameters at ~1 µm were as follows: modulation depth of 0.6%, non-saturable loss of 0.4%, saturation fluence of 70 µJ/cm^2 and time constant of ~1 ps. In order to compensate for the material dispersion from the laser crystal and to balance the self-phase

Optics EXPRESS

modulation (SPM), two flat dispersive mirrors (DM_1 = -250 fs^2 and DM_2 = -150 fs^2) were implemented in the other cavity arm for soliton-like pulse shaping. The physical cavity length of the ML Yb:Ca(Gd,Y)AlO_4 laser was 2.27 m, corresponding to a pulse repetition rate of ~65.9 MHz.

5. Continuous-wave laser operation

The maximum CW output power of the diode-pumped Yb:Ca(Gd,Y)AlO_4 laser reached 347 mW at 1052.5 nm with a 4.5% OC at an absorbed pump power (P_{abs}) of 887 mW, corresponding to an optical efficiency of 39.1% and a slope efficiency (η) of 48.9%, see Fig. 8(a). The laser threshold gradually increased with T_{OC}, from 102 mW (T_{OC} = 0.4%) to 239 mW (T_{OC} = 7.5%). The laser wavelength experienced a monotonous blue-shift with increasing T_{OC} in the range of 1033.3 – 1062.7 nm, as shown in Fig. 8(b). This represents a typical quasi-three-level laser behavior with inherent reabsorption at the laser wavelength.

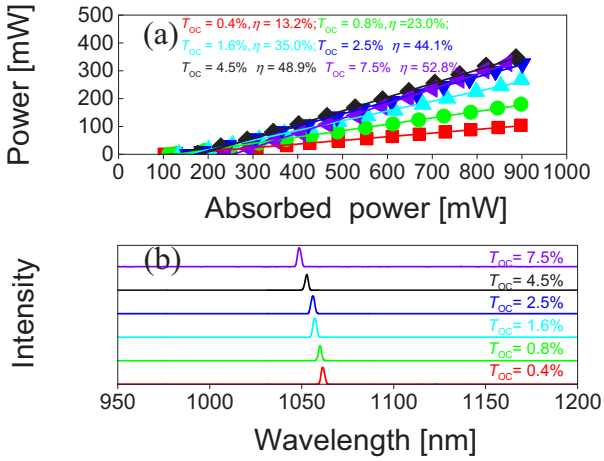

Fig. 8. Diode-pumped Yb:Ca(Gd,Y)AlO_4 laser in the CW regime: (a) input - output dependences for different OCs, η – slope efficiency; (b) Laser spectra measured well above the laser threshold. The laser polarization is $\boldsymbol{E} \perp \boldsymbol{c}$ (σ).

The Caird analysis [32] was employed by fitting the measured laser slope efficiency as a function of the OC, R_{OC} = 1 - T_{OC}. This method allows an estimation of the total round-trip cavity losses δ (excluding reabsorption losses) and the intrinsic slope efficiency η_0, considering the mode-matching and quantum efficiencies. The fit yielded η_0 = 68.2 ± 0.25% and δ = 1.33 ± 0.15%, as illustrated in Fig. 9(a).

The wavelength tuning of the Yb:Ca(Gd,Y)AlO_4 laser in the CW regime was studied by introducing a 2-mm thick quartz plate as a Lyot filter at Brewster's angle in the cavity arm terminated by the OC. The laser wavelength was continuously tunable in the range of 1012 -1097 nm, spanning 85 nm at the zero-power-level, for T_{OC} = 1.1% at an incident pump power of 1.33 W. A slightly broader tuning range of 88 nm (1012 – 1100 nm) was observed for T_{OC} = 0.4% at the same pump level. Finally, the maximum tuning range of 90 nm (1010 – 1100 nm) was achieved using a yet lower 0.2% OC, as shown in Fig. 9(b).

Optics EXPRESS

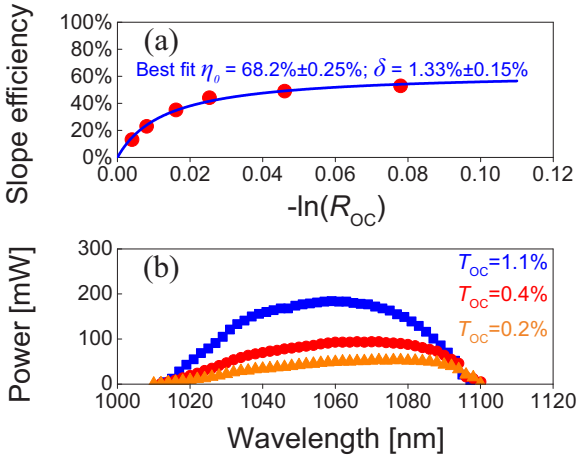

Fig. 9. CW diode-pumped Yb:Ca(Gd,Y)AlO_4 laser: (a) Caird analysis: slope efficiency *vs.* the OC reflectivity $R_{OC} = 1 - T_{OC}$; (b) wavelength tuning curves obtained with a Lyot filter and three OCs (0.2% - 1.1%). The laser polarization is $\boldsymbol{E} \perp \boldsymbol{c}$ (σ).

6. Mode-locked laser operation

Self-starting ML operation was initiated and stabilized by implemented a SESAM. Two DMs were introduced into the laser cavity, providing an overall negative GDD of -1600 fs^2 for soliton-like pulse shaping, refer to Fig. 7. The spectral and temporal characteristics of the ML Yb:Ca(Gd,Y)AlO_4 laser are depicted in Fig. 10. Using a 2.5% OC, the ML laser delivered pulses with a spectral bandwidth of 31.3 nm (FWHM) at a central wavelength of 1063.5 nm, assuming a $sech^2$-shaped spectral profile, see Fig. 10(a). The second-harmonic generation (SHG)-based background-free intensity autocorrelation trace (AC) was well-fitted with a $sech^2$-shaped temporal profile, resulting in an estimated pulse duration of 42 fs (FWHM) and a time-bandwidth-product (TBP) of 0.348, slightly higher compared to the Fourier-transform-limited value (0.315), see Fig. 10(b). Excellent $sech^2$-shaped spectral and temporal profiles indicating soliton-like ML pulses were achieved. An average output of 105 mW was achieved at 60 MHz for a P_{abs} of 827 mW, corresponding to a peak power of 36.7 kW. The inset in Fig. 10(b) displays the measured SHG-based background-free intensity AC over a long-time span of 50-ps, indicating single-pulse CW-ML operation free of multiple pulse instabilities.

The generation of shortest pulses with optimal stability was achieved using the 1.6% OC. The self-starting nature of the ML Yb:Ca(Gd,Y)AlO_4 laser was reaffirmed. The characterization of these shortest pulses is succinctly presented in Fig. 11. The measured optical spectrum of the shortest pulses exhibited an emission bandwidth (FWHM) of 38.3 nm, assuming a $sech^2$-shaped spectral intensity profile at a central wavelength of 1059.8 nm, see Fig. 11(a). The measured intensity autocorrelation trace yielded a deconvolved pulse duration of 35 fs (FWHM) when assuming a $sech^2$-shaped temporal profile; see Fig. 11(b). The corresponding TBP of 0.358 was above the Fourier-transform-limited value (0.315) indicating a certain chirp. The inset in Fig. 11(b) shows the measured intensity autocorrelation trace over a long-time span of 50 ps, indicating single-pulse CW-ML operation free of multiple pulse instabilities. An average output power of 51 mW was obtained for an absorbed pump power of 845 mW, with a pulse repetition rate of 65.95 MHz, corresponding to a peak power of 19.4 kW.

The confirmation of ML operation stability was achieved by recording the radio-frequency (RF) spectra of the shortest pulses over various frequency ranges, as illustrated in Fig. 12. The fundamental beat note at 65.95 MHz displayed a substantial extinction ratio, exceeding 75

Optics EXPRESS

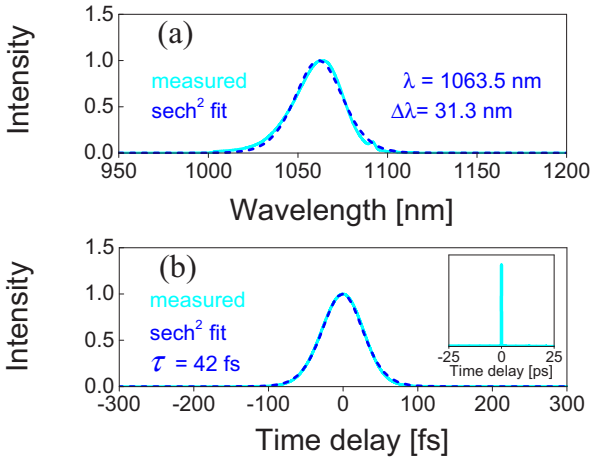

Fig. 10. Diode-pumped SESAM ML Yb:Ca(Gd,Y)AlO_4 laser with $T_{OC} = 2.5\%$. (a) Laser spectrum and (b) Recorded SHG-based autocorrelation trace. *Inset* in (b) simultaneously measured long-scale (50 ps) autocorrelation trace.

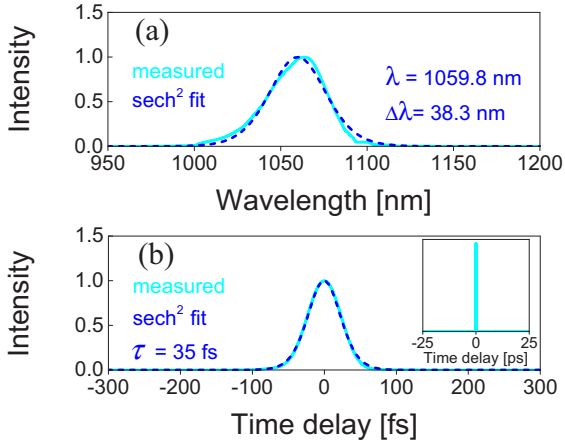

Fig. 11. Diode-pumped SESAM ML Yb:Ca(Gd,Y)AlO_4 laser with $T_{OC} = 1.6\%$. (a) Laser spectrum and (b) Recorded SHG-based autocorrelation trace. *Inset* in (b) simultaneously measured long-scale (50 ps) autocorrelation trace.

Optics EXPRESS

dBc above the carrier, see Fig. 12(a). Furthermore, the measured uniform harmonics across a 1-GHz frequency span emphasized the remarkable stability of the single-pulse ML operation, see Fig. 12(b).

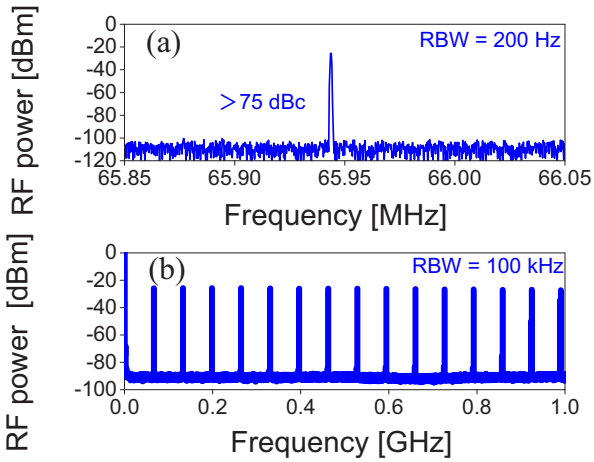

Fig. 12. RF spectra of the SESAM ML Yb:Ca(Gd,Y)AlO_4 laser: (a) Fundamental beat note at 65.95 MHz recorded with a resolution bandwidth (RBW) of 200 Hz, and (b) Harmonics on a 1-GHz frequency span recorded with an RBW of 100 kHz. T_{OC} = 1.6%.

To validate the pulse shaping mechanism, the far-field beam profiles of the diode-pumped Yb:Ca(Gd,Y)AlO_4 laser were recorded using an infrared (IR) camera positioned at approximately 0.8 m from the OC. The transition between the CW and ML regimes was easily achieved through a slight cavity misalignment. Notably, minimal changes in the far-field beam diameter were observed during such a transition, as depicted in Fig. 13. This observation, coupled with the almost perfect $sech^2$-shaped spectral and temporal profiles of the shortest laser pulses, indicates that soliton mode-locking stabilized by the SESAM was the dominant pulse shaping mechanism.

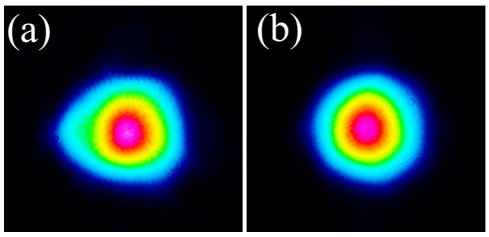

Fig. 13. Measured far-field beam profiles of the diode-pumped SESAM ML Yb:Ca(Gd,Y)AlO_4 laser: (a) CW and (b) SESAM ML operation regimes.

7. Conclusion

In summary, this work reports on the growth, spectroscopic characterization, and the first continuous-wave and passively mode-locked laser operation of a novel "mixed" disordered calcium aluminate crystal, Yb^{3+}-doped Ca(Gd,Y)AlO_4. The tetragonal structure of the stoichiometric compounds is preserved but the mixed host induces additional spectral broadening for the Yb^{3+} absorption and emission bands. Consequently, it becomes an appealing material for generating sub-50 fs pulses from mode-locked lasers at ~1 µm. The laser performance was studied using a ***c***-cut Yb:Ca(Gd,Y)AlO_4 crystal pumped by a spatially single-mode, 976-nm fiber-coupled

Optics EXPRESS

laser diode. In the continuous-wave regime, a maximum output power of 347 mW was achieved at 1052.5 nm with a slope efficiency of 48.9%. Continuous wavelength tuning across 90 nm (1010 – 1100 nm) was obtained using a quartz-based Lyot filter. By employing a commercial SESAM to start and sustain the mode-locked operation, the Yb:Ca(Gd,Y)AlO_4 laser generated soliton pulses as short as 35 fs at 1059.8 nm with an average output power of 51 mW, operating at ~65.95 MHz. The average output power can be scaled to 105 mW with a slightly longer pulses of 42 fs at 1063.5 nm. Further pulse shortening and average output power scaling could be achieved by soft-aperture Kerr-lens mode-locking.

Funding. National Natural Science Foundation of China (62375106, 51972149, 61975208, U21A20508); Sino-German Scientist Cooperation and Exchanges Mobility Program (M-0040); Science and Technology Program of Guangzhou (2024A03J0240); Ministerio de Ciencia e Innovación (MCIN/AEI/10.13039/501100011033, PID2022-141499OB-I00, PID2019-108543RB-I00).

Acknowledgment. Xavier Mateos acknowledges the Serra Húnter program.

Disclosures. The authors declare no conflicts of interest.

Data availability. Data underlying the results presented in this paper are not publicly available at this time but may be obtained from the authors upon reasonable request.

References

1. W. Tian, X. Tian, Q. Li, *et al.*, "Kerr-lens mode-locked femtosecond Yb:CALYO oscillator with more than 20-W average power," Opt. Lett. **48**(18), 4789–4792 (2023).
2. A. Greborio, A. Guandalini, and J. Aus der Au, "Sub-100 fs pulses with 12.5-W from Yb:CALGO based oscillators," Proc. SPIE **8235**, 823511–823516 (2012).
3. W. Tian, R. Xu, L. Zheng, *et al.*, "10-W-scale Kerr-lens mode-locked Yb:CALYO laser with sub-100-fs pulses," Opt. Lett. **46**(6), 1297–1300 (2021).
4. P. Loiko, J. M. Serres, X. Mateos, *et al.*, "Microchip Yb:$CaLnAlO_4$ lasers with up to 91% slope efficiency," Opt. Lett. **42**(13), 2431–2434 (2017).
5. P. Sévillano, P. Georges, F. Druon, *et al.*, "32-fs Kerr-lens mode-locked Yb:$CaGdAlO_4$ oscillator optically pumped by a bright fiber laser," Opt. Lett. **39**(20), 6001–6004 (2014).
6. F. Pirzio, S. D. D. D. Cafiso, M. Kemnitzer, *et al.*, "Sub-50-fs widely tunable Yb:$CaYAlO_4$ laser pumped by 400-mW single-mode fiber-coupled laser diode," Opt. Express **23**(8), 9790 - 9795 (2015).
7. A. Agnesi, A. Greborio, F. Pirzio, *et al.*, "40-fs Yb^{3+}:$CaGdAlO_4$ laser pumped by a single-mode 350-mW laser diode," Opt. Express **20**(9), 10077–10082 (2012).
8. W. Tian, G. Wang, D. Zhang, *et al.*, "Sub-40-fs high-power Yb:CALYO laser pumped by single-mode fiber laser," High Power Laser Sci. Eng. **7**, e64 (2019).
9. J. Ma, H. Huang, K. Ning, *et al.*, "Generation of 30 fs pulses from a diode-pumped graphene mode-locked Yb:$CaYAlO_4$ laser," Opt. Lett. **41**(5), 890–893 (2016).
10. Z. Gao, J. Zhu, J. Wang, *et al.*, "Generation of 33 fs pulses directly from a Kerr-lens mode-locked Yb:$CaYAlO_4$ laser," Photonics Res. **3**(6), 335–338 (2015).
11. S. Kimura, S. Tani, and Y. Kobayashi, "Raman-assisted broadband mode-locked laser," Sci. Rep. **9**(1), 3738 (2019).
12. F. Labaye, V. J. Wittwer, M. Hamrouni, *et al.*, "Efficient few-cycle Yb-doped laser oscillator with Watt-level average power," Opt. Express **30**(2), 2528–2538 (2022).
13. N. Modsching, C. Paradis, F. Labaye, *et al.*, "Kerr lens mode-locked Yb:CALGO thin-disk laser," Opt. Lett. **43**(4), 879–882 (2018).
14. S. Manjooran and A. Major, "Diode-pumped 45 fs Yb:CALGO laser oscillator with 1.7 MW of peak power," Opt. Lett. **43**(10), 2324–2327 (2018).
15. Y. Wang, X. Su, Y. Xie, *et al.*, "17.8 fs broadband Kerr-lens mode-locked Yb:CALGO oscillator," Opt. Lett. **46**(8), 1892–1895 (2021).
16. J. Ma, F. Yang, W. Gao, *et al.*, "Sub-five-optical-cycle pulse generation from a Kerr-lens mode-locked Yb:$CaYAlO_4$ laser," Opt. Lett. **46**(10), 2328–2331 (2021).
17. J. Petit, P. Goldner, and B. Viana, "Laser emission with low quantum defect in Yb:$CaGdAlO_4$," Opt. Lett. **30**(11), 1345–1347 (2005).
18. P. Loiko, F. Druon, P. Georges, *et al.*, "Thermo-optic characterization of Yb:$CaGdAlO_4$ laser crystal," Opt. Mater. Express **4**(11), 2241–2249 (2014).
19. F. Druon, M. Olivier, A. Jaffrès, *et al.*, "Magic mode switching in Yb:$CaGdAlO_4$ laser under high pump power," Opt. Lett. **38**(20), 4138–4141 (2013).
20. X. Niu, H. Chen, P. Zhang, *et al.*, "Novel laser crystal Nd^{3+}:Ca(Y,Gd)AlO_4: A promising candidate for laser operation beyond 1.37 μm," J. Alloys Compd. **938**, 168613 (2023).
21. Q. Hu, X. Su, Y. Wang, *et al.*, "Spectroscopic properties and ultrafast performance of Yb:$CaLu_xGd_{1-x}AlO_4$ crystal," Laser Phys. Lett. **14**(4), 045809 (2017).

Optics EXPRESS

22. Z. Pan, P. Loiko, J. M. Serres, *et al.*, ""Mixed" Tm:Ca(Gd,Lu)AlO4 – A novel crystal for tunable and mode-locked 2 µm lasers," Opt. Express **27**(7), 9987–9995 (2019).
23. Z. Pan, P. Loiko, S. Slimi, *et al.*, "Tm,Ho:Ca(Gd,Lu)AlO_4 crystals: Crystal growth, structure refinement and Judd-Ofelt analysis," J. Lumin. **246**, 118828 (2022).
24. C. Liebald, "Yb-dotierte Ultrakurzpuls-Lasermaterialien mit K_2NiF_4-Struktur - Züchtung und Verbesserung der Kristallqualität," (Doctoral dissertation, Johannes Gutenberg-Universität Mainz, 2017) [in German].
25. J. Di, X. Xu, C. Xia, *et al.*, "Crystal growth, polarized spectra, and laser performance of Yb:$CaGdAlO_4$ crystal," Laser Phys. **26**(4), 045803 (2016).
26. D. Li, X. Xu, Y. Cheng, *et al.*, "Crystal growth and spectroscopic properties of Yb:$CaYAlO_4$ single crystal," J. Cryst. Growth **312**(14), 2117–2121 (2010).
27. D. L. Rousseau, R. P. Bauman, and S. P. S. Porto, "Normal mode determination in crystals," J. Raman Spectrosc. **10**(1), 253–290 (1981).
28. V. G. Hadjiev, M. Cardona, I. Ivanov, *et al.*, "Optical phonons probe of the $SrLaAlO_4$ crystal structure," J. Alloys Compd. **251**(1-2), 7–10 (1997).
29. T. C. Damen, S. P. S. Porto, and B. Tell, "Raman effect in zinc oxide," Phys. Rev. **142**(2), 570–574 (1966).
30. P. Loiko, P. Becker, L. Bohatý, *et al.*, "Sellmeier equations, group velocity dispersion, and thermo-optic dispersion formulas for $CaLnAlO_4$ (Ln = Y, Gd) laser host crystals," Opt. Lett. **42**(12), 2275–2278 (2017).
31. J. A. Hutchinson, H. R. Verdun, B. H. Chai, *et al.*, "Spectroscopic evaluation of $CaYAlO_4$ doped with trivalent Er, Tm, Yb and Ho for eyesafe laser applications," Opt. Mater. **3**(4), 287–306 (1994).
32. J. A. Caird, S. A. Payne, P. R. Staver, *et al.*, "Quantum electronic properties of the $Na_3Ga_2Li_3F_{12}:Cr^{3+}$ laser," IEEE J. Quantum Electron. **24**(6), 1077–1099 (1988).